THE ASTROPHYSICAL JOURNAL, 439:121–131, 1995 January 20

EXTENDED SOFT X-RAY EMISSION IN SEYFERT GALAXIES: *ROSAT* HRI OBSERVATIONS OF NGC 3516, NGC 4151, AND MARKARIAN 3

JON A. MORSE AND ANDREW S. WILSON
Space Telescope Science Institute, 3700 San Martin Drive, Baltimore, MD 21218; morsey@stsci.edu, awilson@stsci.edu
MARTIN ELVIS
Harvard-Smithsonian Center for Astrophysics, 60 Garden Street, Cambridge, MA 02138; elvis@cfa.harvard.edu
AND
KIMBERLY A. WEAVER
Department of Astronomy and Astrophysics, 525 Davey Laboratory, Penn State University, University Park, PA 16802; kweaver@astro.psu.edu
Received 1994 May 26; accepted 1994 July 28

ABSTRACT

We have used the *ROSAT* High Resolution Imager (HRI) to examine the distribution of soft X-rays in three nearby Seyfert galaxies with $\sim 4''$–$5''$ FWHM spatial resolution. A feature of our analysis is an attempt to remove errors in the aspect solution using a method developed by one of us (J. M.).

NGC 4151 shows resolved X-ray emission that is spatially correlated with the optical extended narrow-line region (ENLR), confirming the results obtained with the *Einstein* HRI by Elvis, Briel, & Henry. Image deconvolutions allow us to trace the extended X-rays along a position angle of $\sim 50°/230°$ as far as ~ 1.5 kpc southwest and ~ 0.5 kpc northeast of the nucleus (assuming a distance of 20 Mpc with $H_0 = 50$ km s^{-1} Mpc^{-1}). When a point source is subtracted from the nucleus of NGC 4151, the extended, bipolar X-rays peak in brightness ~ 425 pc southwest of the nucleus and ~ 280 pc northeast of the nucleus. The extended emission accounts for at least 31% of the total 0.1–2 keV *ROSAT* HRI flux (19% from the southwest quadrant, 12% from the northeast and constitutes roughly half of the total soft X-ray excess emission observed with other X-ray detectors. The soft X-ray excess in NGC 4151 has been modeled recently as containing both variable and constant flux components. We suggest that the constant flux component of the soft excess emission originates in the spatially extended regions we have resolved. If the extended X-rays result from electron-scattering of nuclear X-rays, the central source must emit anisotropically, and preferentially toward the extended X-rays and the ENLR. Alternatively, the extended X-rays may represent thermal emission from a hot ($T \sim 10^7$ K), outflowing wind which is in rough pressure equilibrium with the optical narrow-line–emitting clouds observed over the same spatial scale.

NGC 3516 is elongated along a position angle of $\sim 40°/220°$, similar to the direction of the Z-shaped narrow-line region. However, the azimuthally averaged radial brightness profile inside a radius of $10''$ is not distinguishable from a calibration point source. Much or all of the elongation may result from residual errors in the aspect solution, although an extended component associated with the ENLR is possible.

Mrk 3 is very faint in our HRI image and is probably spatially unresolved. We detect the faint X-ray source $\sim 2'$ west of the Mrk 3 nucleus previously found by Turner, Urry, & Mushotzky. It is not known whether this companion is physically associated with Mrk 3 although it does lie along a direction that is within $\simeq 1°$ of the axis of the $2''$ nuclear radio jet.

We also detected the BL Lac object BL 1207+39 $\sim 5'$ north-northwest of NGC 4151. This object appears spatially unresolved, but some excess X-ray emission may be observed in the azimuthally averaged radial brightness profile of BL 1207+39 between radii of $10''$ and $30''$ when compared to a calibration source. A much deeper image is necessary to confirm this result.

Subject headings: galaxies: individual (NGC 3516, NGC 4151, Markarian 3) — galaxies: Seyfert — X-rays: galaxies

1. INTRODUCTION

Spatially extended X-ray emission may be a common feature among Seyfert galaxies (Elvis et al. 1990; Wilson et al. 1992; see Wilson 1994 for an overview). This is not surprising since high-velocity outflows from active galactic nuclei (AGNs) should generate hot gas behind shock waves that form in wind-cloud interactions or through entrainment of interstellar gas by the nuclear-driven jet. Gas may be heated to soft X-ray–emitting temperatures by the compact nuclear UV–X-ray source. Synchrotron emission or inverse Compton scattering by relativistic electrons may also produce extended X-rays. In addition, X-rays generated in the compact active nucleus may be scattered by circumnuclear electrons and be seen as an X-ray "halo." AGN outflows and nuclear radiation fields are often observed to be collimated, so any of the above mechanisms may generate extended X-ray distributions as well.

The interpretation of soft X-ray spectra and time variability of AGNs will be complicated by the presence of spatially extended X-rays. The spectra may reflect a composite of emission mechanisms and X-rays produced from outlying regions will "dilute" any variability of the compact source. It is valuable, therefore, to map the spatial structure of the X-ray–

emitting regions in nearby active galaxies at the highest spatial resolution possible.

We have begun a program to image nearby Seyfert galaxies with a resolution of $\sim 4''$–$5''$ using the *ROSAT* High Resolution Imager (HRI) in order to resolve the spatial structure of hot gas that may be associated with the narrow-line regions (NLRs), extended narrow line regions (ENLRs), and radio sources in these galaxies. This paper reports our HRI observations of two Seyfert 1 galaxies, NGC 3516 and NGC 4151, and a Seyfert 2 galaxy, Markarian 3. HRI observations of other Seyfert galaxies included in this program are discussed elsewhere (NGC 1068, Wilson et al. 1992; NGC 2110, Weaver et al. 1994b; NGC 4258, Cecil, Wilson, & DePree 1994).

2. OBSERVATIONS AND RESULTS

2.1. *ROSAT HRI Observations*

We observed the three Seyfert galaxies in the 0.1–2 keV energy range with the *ROSAT* HRI for between 9 ks and 19 ks (Table 1). Each source was observed on-axis and was detected within $2''$ of the known optical and radio position of the Seyfert nucleus. A moderately bright BL Lac object, BL 1207+39, was also detected $\sim 5'$ north–northwest of NGC 4151.

Each HRI image combines data recorded over several satellite orbital intervals (or OBIs). The count rate for each source was determined by extracting counts from a $1'$ radius circle centered on the source. Beyond $1'$ the radial brightness profiles are dominated by noise. Background counts were culled from a $2'.5$ wide annulus outside a radius of $4'$ from the source center. For the source pair NGC 4151 and BL 1207+39, a wedge-shaped region of 75° half-angle toward the other source was excluded from the background region. The background count rates were consistent with expectations (David et al. 1993). Table 1 summarizes the details of the observations.

2.2. *The Search for Extended Emission*

The intrinsic spatial resolution of $4''$–$5''$ FWHM of the *ROSAT* X-Ray Telescope (XRT) plus HRI is blurred by errors in the knowledge of the pointing position of the telescope as a function of time (the "aspect solution"). These errors in the aspect solution complicate the identification of extended X-ray emission within $\sim 10''$ of bright, unresolved central sources (David et al. 1993). Aspect errors may cause elongations in point sources and lead to inflated azimuthally averaged radial brightness profiles. Weak, extended X-ray emission in the circumnuclear regions of Seyfert galaxies may also cause these sources to appear elongated or inflated in the HRI images (e.g., Elvis et al. 1990), so it is necessary to attempt to correct for aspect errors before deciding whether any apparent extensions represent real extended emission. We have developed a method to evaluate and correct errors in the aspect solution in HRI observations of compact sources (Morse 1994a, b), which we summarize below.

Every X-ray photon detected by the HRI is timed and assigned a position on the detector (see Zombeck et al. 1990). The aspect solution provides a conversion from detector position to celestial coordinates as a function of time based on the pointing map provided by the XRT star tracker. HRI observations are normally wobbled along a direction $\sim 45°$ clockwise with respect to the roll angle through a full amplitude of several arcminutes in order to smooth out quantum efficiency variations across the detector; the source is thus swept across a $\gtrsim 400$ pixel range on the detector during an observation. In addition, individual OBIs generally do not exceed ~ 3600 s in duration, so photons detected from several OBIs are normally combined to achieve the final image. Aspect errors may be manifest as broadenings or elongations caused by systematic offsets between different OBIs or as a function of phase in the wobble. Point sources do not always appear broadened or elongated in HRI observations; sometimes the tracking is excellent and point sources appear perfectly round and consistent with the expected XRT + HRI point spread function. Errors in the aspect solution vary from observation to observation (even of the same source) in an unpredictable way (David et al. 1993). The position angles of apparent elongations of many point sources are uncorrelated with the direction of the satellite wobble.

To map out aspect errors in HRI observations of unresolved sources, one would ideally like to monitor the source centroid over very short time intervals and apply corrections to the original aspect solution as a function of time. Such a procedure has been used by Schmitt, Güdel, & Predehl (1994) to reconstruct point sources. However, all of the targets discussed in the present paper have count rates significantly less than 1 count s^{-1} and do not accrue sufficient counts to achieve accurate image centroids in short time intervals. The source moves ~ 2 pixels ($=1''$) per second across the detector during the wobble, so even subimages containing photons recorded over time intervals as short as 30 s may exhibit elongations.

We correct for aspect errors in two steps. First, we fold the data in time to check whether there are any systematic offsets between the different OBIs of an observation. Second, we create subimages from small regions in *detector coordinates* through which the source passed while the satellite was wobbled. The subimages contain photons recorded at a given phase during multiple cycles of the wobble. We thus assume

TABLE 1

ROSAT HRI OBSERVATIONS

Object	Date	"Live Time" (s)	HRI Counts[a]	HRI Counts s^{-1}	Background[b]	Hardness Ratio[c]
NGC 3516	1992 Apr 18–21	17913	5938 ± 80	0.332 ± 0.004	1.27×10^{-6}	0.64 ± 0.02
NGC 4151	1993 May 17	9163	1777 ± 45	0.194 ± 0.005	1.34×10^{-6}	0.26 ± 0.02
Mrk 3	1992 Mar 12–14	19315	449 ± 28	0.023 ± 0.001	1.12×10^{-6}	0.81 ± 0.11
BL 1207+39.....	1993 May 17	9163	872 ± 33	0.095 ± 0.004	1.31×10^{-6}	0.58 ± 0.05

[a] Net counts after background subtraction, extracted from circular regions with radii of $1'$ centered on the nucleus of each source.

[b] In counts s^{-1} $arcsec^{-2}$. Background counts were extracted from annuli with inner radii of $4'$ and widths of $2'.5$ centered on the nucleus of each source. The background regions for NGC 4151 and BL 1207+39 excluded a wedge-shaped region of 75° half-angle in the direction toward the other source.

[c] Hardness ratio equals the number of HRI counts in PHA channels 5–10 divided by the number of counts in channels 1–4. Harder spectra have higher ratios.

that the aspect errors are systematic as a function of wobble phase. These data segments are reimaged in sky coordinates, aligned to a common center, and co-added. Photons detected far from the source center are excluded in this correction scheme, which is designed to aid the detection of extended X-ray emission within $\sim 10''$ of a compact source.

2.2.1. *NGC 3516*

The nearby Seyfert 1 galaxy NGC 3516 shows extended emission in the optical and radio wavebands over scales of $\sim 2''$–$15''$ from the active nucleus (e.g., Miyaji, Wilson, & Pérez-Fournon 1992). The NLR of this object curves outward from the nucleus in opposite directions, giving it a Z-shaped appearance (Pogge 1989). These filaments exhibit a velocity field suggestive of a bipolar outflow (Goad & Gallagher 1987; Mulchaey et al. 1992; Veilleux, Tully, & Bland-Hawthorn 1993). High-resolution 6 and 20 cm radio observations (Miyaji et al. 1992) show a core/jet structure that is cospatial with the extended optical line emission to the northeast of the nucleus. Lower resolution 6 cm radio maps by Wrobel & Heeschen (1988) reveal faint, diffuse emission that is aligned with the optical line emission on both sides of the nucleus. The existing data suggest that a nuclear-driven jet is interacting with the circumnuclear medium.

After processing with the standard aspect solution, the HRI image of NGC 3516 is elongated along a position angle (PA) of $\sim 40°$, roughly aligned with the extended Z-shaped narrow-lined optical emission. We compared our HRI image of NGC 3516 to a known point source to ascertain whether the elongation represents real extended emission. Unfortunately, there is no suitable point source in the HRI image itself, so we had to use a separate high signal-to-noise, on-axis HRI image of the soft X-ray point source HZ 43 (supplied to us by Dr. Larry David). Figure 1 compares the azimuthally averaged radial brightness profiles measured from the original NGC 3516 and HZ 43 images. We used the 2 Gaussian plus exponential parameterization of David et al. (1993) to match the radial profile of HZ 43, and then scaled this fit to compare with the NGC 3516 profile. The NGC 3516 profile is well matched by the fit inside a radius of $10''$, but there may be some excess emission between radii of $10''$ and $30''$.

We applied the aspect error correction method described above to determine whether the elongation inside a radius of $10''$ results from aspect errors or real extended X-ray emission. We found no significant OBI-to-OBI systematic shifts in the aspect solution for the observation of NGC 3516. However, the image centroid showed clear offsets from a mean position as a function of wobble phase. Figure 2 shows the distribution of offsets for the 20 subimages we created; these offsets lie approximately along the direction of the elongation in the original image. After translating the subimages to a common center and co-adding them into a single image, the resulting image has a narrower and more symmetric core than in the original image (Fig. 3). Some asymmetries remain at low flux levels beyond a radius of $\sim 5''$.

We overlay the corrected X-ray image of NGC 3516 on the [O III] image of Miyaji et al. (1992) in Figure 4. The residual elongation in the corrected image aligns with the Z-shaped NLR, but we cannot be certain that all aspect errors have been removed. If we subtract off a circularly symmetric point spread function whose width matches the FWHM along the direction *perpendicular* to the elongation in the corrected image, we find that the extended flux from the Z-shaped NLR is $\lesssim 20\%$ of the total HRI flux.

For comparison with the corrected NGC 3516 image, we applied exactly the same aspect error correction procedure to the HZ 43 observation. The original image of HZ 43 also showed an elongation along roughly the same PA as in NGC 3516, but in this case the ellipticity is almost certainly instrumental in origin. The offsets in the HZ 43 subimage centroids from a mean position were very similar in magnitude to those measured for NGC 3516. In addition, after applying the aspect error correction procedure to HZ 43, there was some asymmetry present in the resultant image of HZ 43 outside a radius of $5''$, which probably may be ascribed to residual aspect errors (see Morse 1994a).

In Figure 5 we compare the azimuthally averaged radial brightness profiles of the uncorrected and corrected images of NGC 3516 with the corrected profile of HZ 43. Based on a comparison to the corrected HZ 43 fit, we find that within

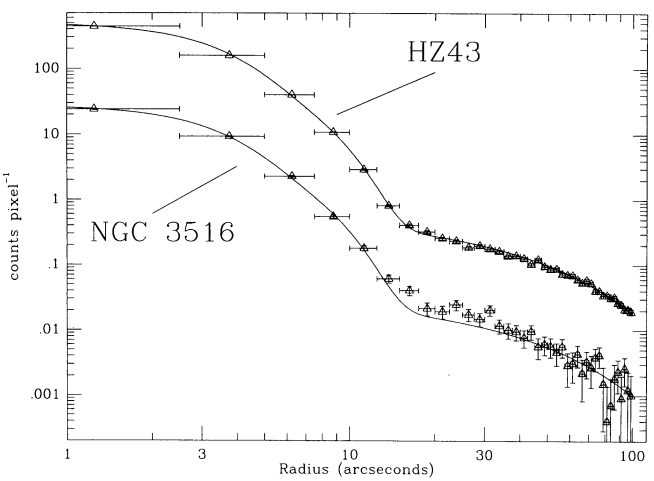

FIG. 1.—The azimuthally averaged radial brightness profiles from the uncorrected HRI images of NGC 3516 and HZ 43. The solid line is a fit to the HZ 43 profile using the 2 Gaussian plus exponential parameterization of David et al. (1993), which has also been scaled to the NGC 3516 profile. Some excess emission may be evident in NGC 3516 between radii of $10''$ and $30''$.

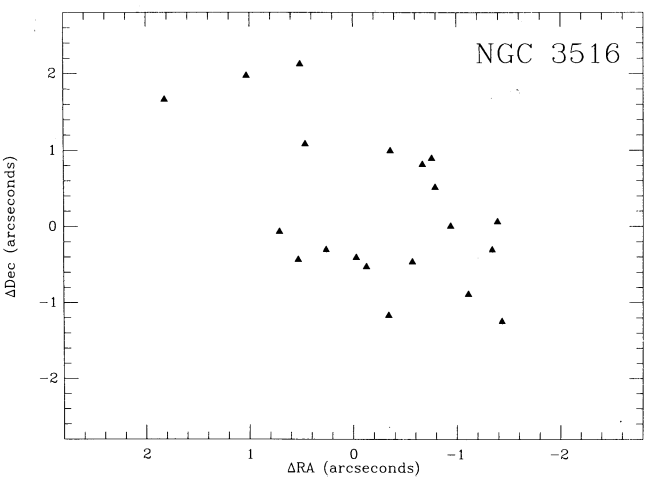

FIG. 2.—The distribution of NGC 3516 subimage centroid offsets in right ascension vs. those in declination. The offsets are aligned roughly with the direction of the ellipticity (PA $\sim 40°$) in the original image.

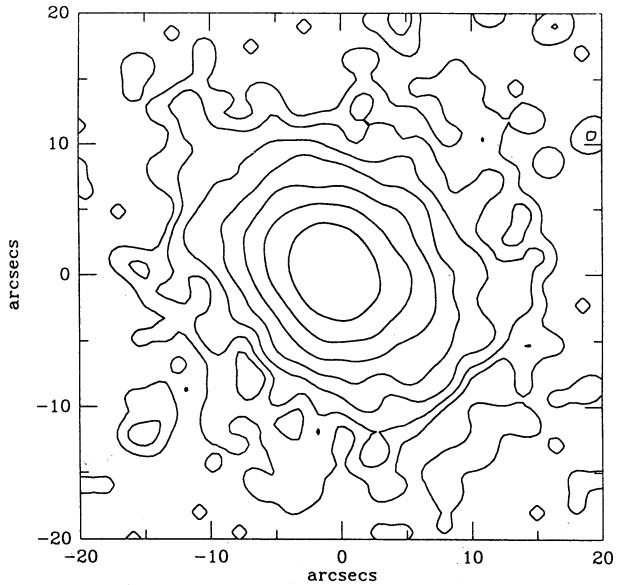

FIG. 3a

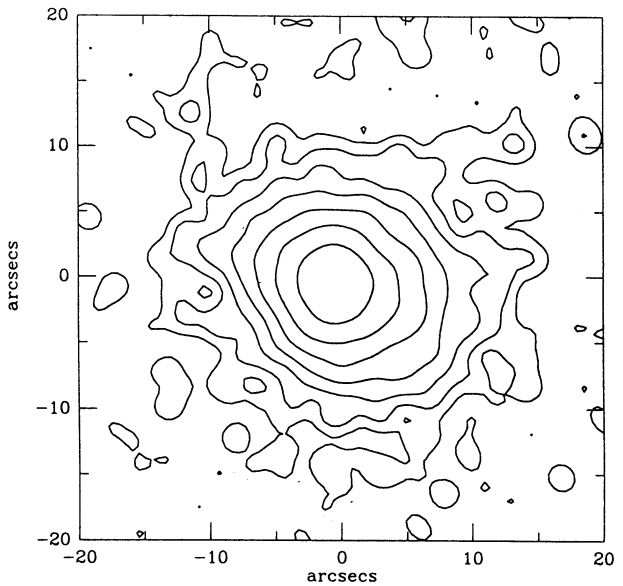

FIG. 3b

FIG. 3.—Contour diagrams of the (*a*) original and (*b*) corrected HRI images of NGC 3516 (see text for details). Each image has been smoothed by a Gaussian with a FWHM of 2″. Contour levels are spaced at factors of 2.512 with respect to the peak intensity in each image. The core of the image in (*b*) is narrower and more symmetric after correcting the image in (*a*) for aspect errors.

~10″ of the image core we cannot distinguish with certainty the X-ray morphology of NGC 3516 from a point source. We must await a better remedy for aspect errors before judging whether the elongation of the core is real or spurious.

2.2.2. *NGC 4151*

The famous nearby galaxy NGC 4151 is one of the best-studied Seyfert galaxies. Recent optical spectroscopy and imaging with the *Hubble Space Telescope* of the nuclear region have revealed broad-line emission emanating from an unresolved, pointlike nuclear component, and narrow-line emission from small "clouds" distributed in a bicone aligned along the northeast–southwest direction (Evans et al. 1993; Boksenberg et al. 1994). The narrow, forbidden-line region extends as far as 30″–40″ asymmetrically to the southwest of the nucleus (e.g., Heckman & Balick 1983; Pérez-Fournon & Wilson 1990).

Elvis, Briel, & Henry (1983) observed NGC 4151 with the *Einstein* HRI and identified extended soft X-ray emission that appears to be associated with the emission-line gas to the southwest of the nucleus. They estimated that the extended X-rays make up ~15% of the total 0.1–3.0 keV flux. Our

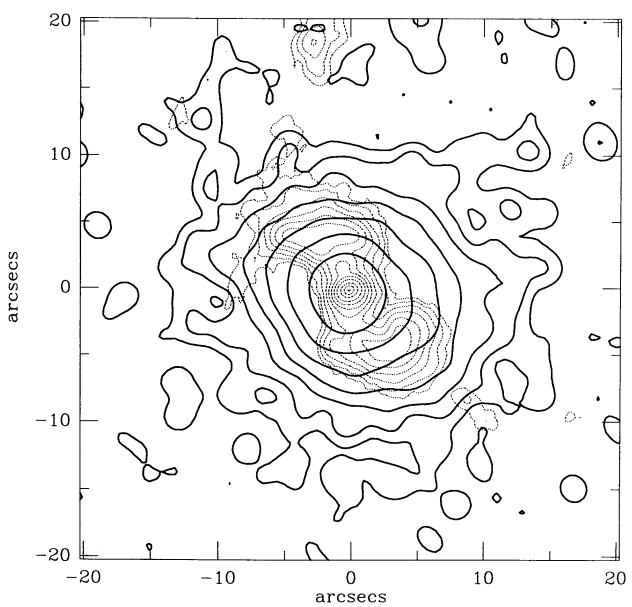

FIG. 4.—Contour diagram of the corrected HRI image of NGC 3516 (*thick lines*) overplotted on the optical [O III] image of Miyaji et al. (1992). The HRI image has been smoothed by a Gaussian with a FWHM of 2″ and the X-ray contour levels are set as in Fig. 3. The X-ray image shows a residual elongation which aligns with the Z-shaped NLR.

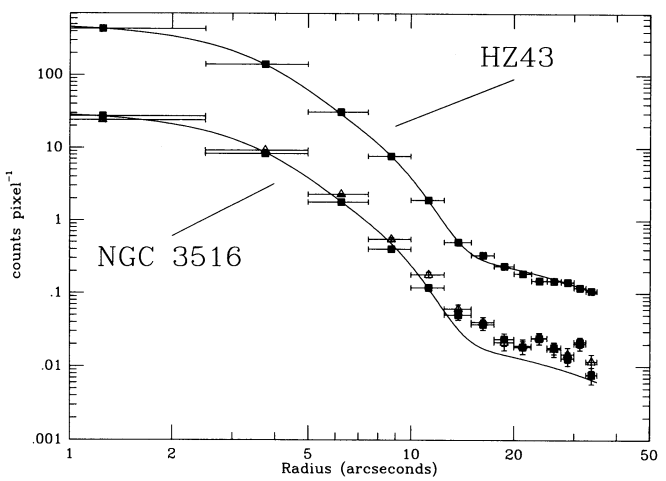

FIG. 5.—The azimuthally averaged radial brightness profiles of the corrected (*filled squares*) and uncorrected (*open triangles*) images of NGC 3516 compared to the corrected HZ 43 image. The solid line is a match to the HZ 43 profile; this line is also plotted after scaling to the peak of the corrected NGC 3516 profile. Despite a residual, apparent elongation in the NGC 3516 HRI image (Fig. 4), we cannot distinguish its azimuthally averaged radial brightness profile from that of a similarly corrected point source.

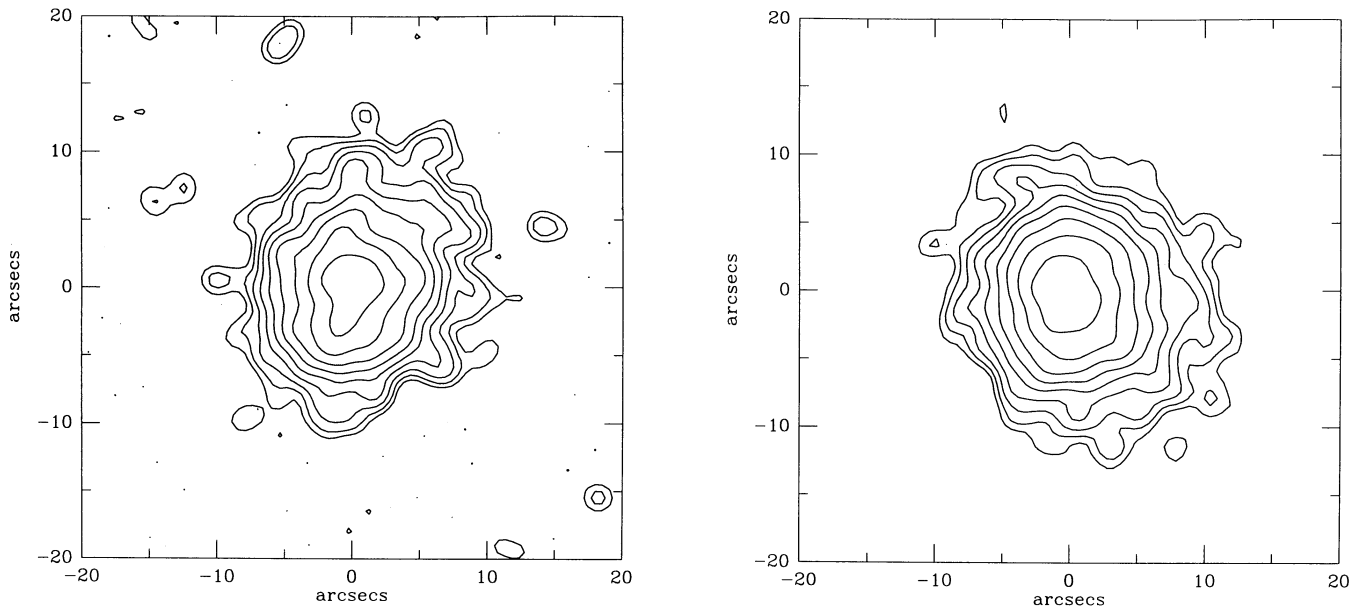

FIG. 6a

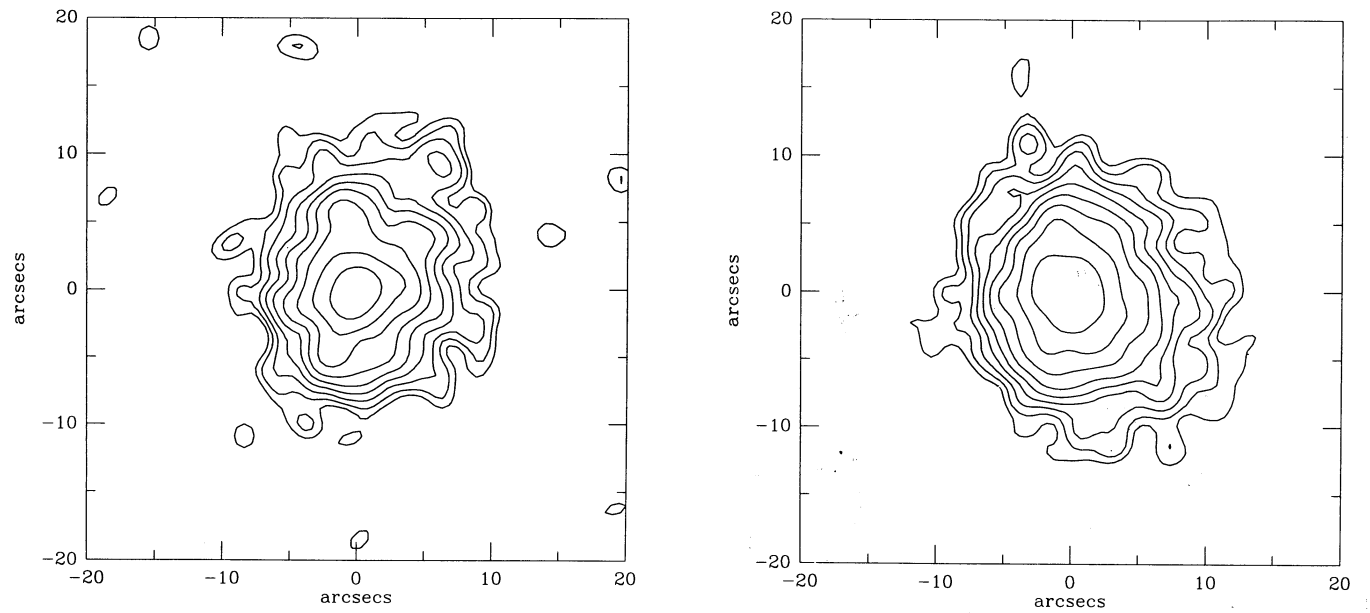

FIG. 6b

FIG. 6.—Contour diagrams of BL 1207+39 (*left*) and NGC 4151 (*right*) from the (*a*) original and (*b*) corrected HRI images. The images have been smoothed by a Gaussian with a FWHM of 2″ and contours are spaced at factors of $(2.512)^{1/2}$ with respect to the maximum intensity in each image.

ROSAT HRI image of NGC 4151 also shows evidence for extended X-ray emission to the southwest of the nucleus, confirming the results of Elvis et al. (1983).

We compared the X-ray distribution in our HRI image of NGC 4151 to that of a pointlike source (identified as the BL Lac object BL 1207+39) ~ 5′ north-northwest of NGC 4151. David et al. (1993) have shown that the HRI point spread function remains essentially unchanged out to off-axis angles of $\lesssim 6'$, beyond which it rapidly enlarges. The images of the two sources are elongated in different directions (Fig. 6*a*), suggesting that part of one or both of the extensions may be real. The NGC 4151 image is elongated in approximately the same direction as found with the *Einstein* HRI (Elvis et al. 1983). In order to search for systematic aspect-related errors between the different OBIs, we examined images of BL 1207+39 from each separate OBI. We found that the source centroid in the first OBI was shifted systematically ~3″ to the south relative to the other three OBIs, which accounts for the double-peaked appearance of the image core of BL 1207+39 in Figure 6*a*. The subimages from each OBI were translated to a common reference and restacked into a single image. The corrected images of BL 1207+39 and NGC 4151 are shown in Figure 6*b*. The large-scale elongations in each source are virtually unaffected by this correction, but the image core of BL 1207+39 is no

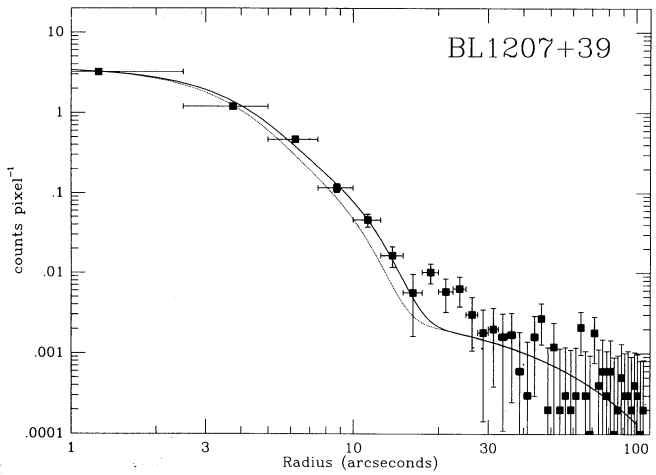

FIG. 7a

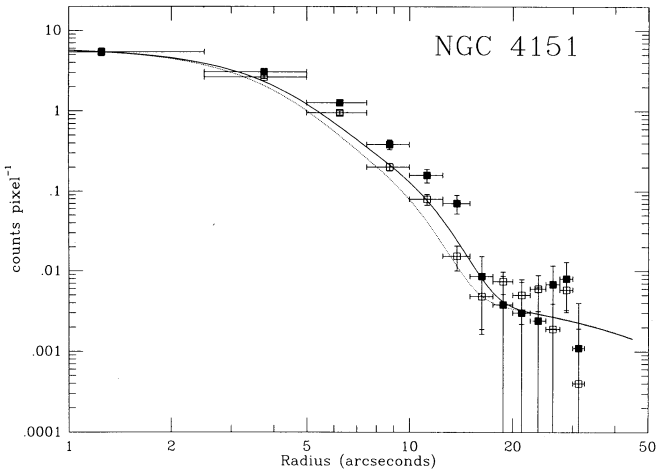

FIG. 7b

FIG. 7.—(*a*) The azimuthally averaged radial brightness profile of BL 1207+39 from the corrected HRI image. The dotted line is the scaled fit to the original HZ 43 image from Fig. 1. The solid curve is a match to the BL 1207+39 profile. (*b*) Radial brightness profiles from the corrected HRI image of NGC 4151. The filled squares are from the southwest quadrant, where most of the extended X-ray emission is seen, and the open squares represent an average profile from the other three quadrants. The dotted and solid lines are the same as in (*a*), scaled to the peak of the NGC 4151 profile. The points plotted extend to only ~35″ radius because of the low signal-to-noise ratios that result from dividing the image into quadrants.

longer double-peaked. Unfortunately, there are too few counts in either source to correct for aspect errors as a function of wobble phase.

Figure 7*a* shows the azimuthally averaged radial brightness profile of the corrected BL 1207+39 image. The dotted line in the plot is the scaled fit to the original on-axis image of HZ 43 (see Fig. 1), using the parameterization of David et al. (1993), while the solid line is a match to the BL 1207+39 profile. The profile of BL 1207+39 appears somewhat inflated compared to the HZ 43 fit within a radius of ~15″, but this could be due to residual, uncorrected aspect errors. The points between radii of 15″ and 30″ that lie well above the plotted curves may indicate the presence of faint spatially extended emission, though we are approaching the noise level in this region. BL 1207+39 has recently been identified with a galaxy cluster at $z = 0.62$ (Q. Wang, private communication) which may contribute to the X-ray emission. A much longer exposure is needed to verify the reality of the extended emission.

In Figure 7*b*, we show radial brightness profiles of the corrected NGC 4151 image from the southwest quadrant (*filled squares*) and the average of the other three quadrants (*open squares*) compared with the fits to HZ 43 and BL 1207+39. All of the points from the southwest quadrant within a radius of ~15″ lie above the points from the other three quadrants as well as above the two curves, suggesting the presence of extended emission in NGC 4151.

A lower limit to the fraction of extended flux in NGC 4151 can be found by scaling the BL 1207+39 image, which we assume is pointlike, to the maximum intensity in NGC 4151 and subtracting it. The residual flux in the southwest quadrant of NGC 4151 is found to be ~19% of the total HRI flux. There is also excess flux in the northeast quadrant, amounting to an additional ~12% of the total flux. Hence, at least ~31% of the total 0.1–2.4 keV flux from NGC 4151 is resolved in our HRI image.

In order to deconvolve the NGC 4151 image, we constructed a model point spread function (PSF) as follows. First, a circularly symmetric PSF was computed from the azimuthally averaged point source radial profile given by David et al. (1993) and used to deconvolve the image of BL 1207+39. The resulting image of BL 1207+39 was almost pointlike with some asymmetry along the north–south direction which we assume is due to aspect errors. Next, this deconvolved image was smoothed with a narrow Gaussian to reduce noise spikes resulting from poor photon statistics. The original, circularly symmetric PSF was then convolved with the processed BL 1207+39 image, the result representing an improved PSF with the aspect errors included. This new PSF was used in deconvolving NGC 4151. (Essentially identical results were obtained by using the image of BL 1207+39 itself as the model PSF.)

Figure 8 (Plate 1) shows a mosaic of original and deconvolved HRI images of BL 1207+39, NGC 4151, and NGC 4151 with the nuclear point source subtracted. All deconvolutions employed 70 iterations of the Lucy-Richardson algorithm. Both the original and the point source–subtracted NGC 4151 images show similar extended morphologies after deconvolution. In the point source–subtracted image, the extended X-rays peak in brightness in the southwest quadrant 4.″4 ± 0.″5 (~425 pc) from the nucleus along a PA of 229° ± 6°. In the northeast quadrant the X-rays peak 2.″9 ± 0.″5 (~280 pc) from the nucleus along a PA of 53° ± 10°. Figure 9 (Plate 2) overlays contours of the extended [O III] λ5007 emission (from Pérez-Fournon & Wilson 1990) on the deconvolved X-ray image of NGC 4151, where we have aligned the emission peaks in the two images. The correspondence between the X-rays and the ENLR is striking. We discuss the flux distribution in NGC 4151 further in § 3.

2.2.3. *Mrk 3*

Mrk 3 is a type 2 Seyfert galaxy with a highly collimated bipolar radio jet (Kukula et al. 1993) that is closely associated with the elongated optical narrow-line region (e.g., Haniff, Wilson & Ward 1988). Miller & Goodrich (1990) detected broad emission lines in the polarized flux spectrum, suggesting the presence of an obscured Seyfert 1 nucleus. The hard X-ray spectrum of Mrk 3 is heavily absorbed (Awaki et al. 1990; Marshall et al. 1991), consistent with the picture that a thick torus is hiding the nucleus from direct view.

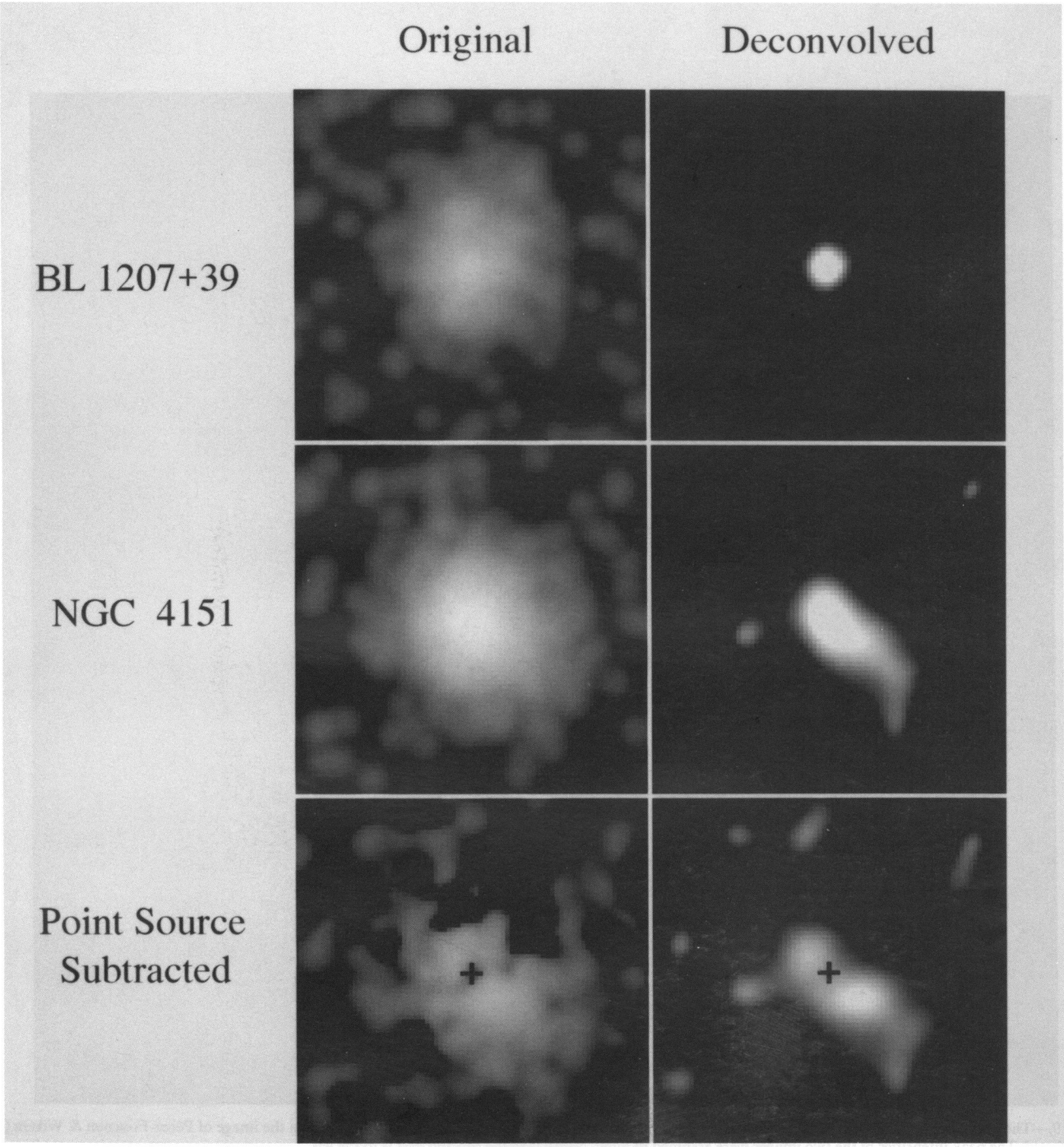

FIG. 8.—Mosaic of HRI images before and after image deconvolutions. The gray scale has a logarithmic stretch. Each individual image is 40″ on a side. North is to the top and east is to the left in each image. The "original" images of BL 1207+39 and NGC 4151 are those shown in Fig. 6*b*. The top two panels show the results for BL 1207+39, which we have assumed is a point source and used to construct a model PSF (see text). The middle two panels show the results for NGC 4151, while the bottom panels show the results when the BL 1207+39 image is scaled and subtracted from the original NGC 4151 image. The cross in each of the bottom two panels marks the position of maximum intensity in the original NGC 4151 image; extended emission is seen to both southwest and northeast of the nucleus.

PLATE 2

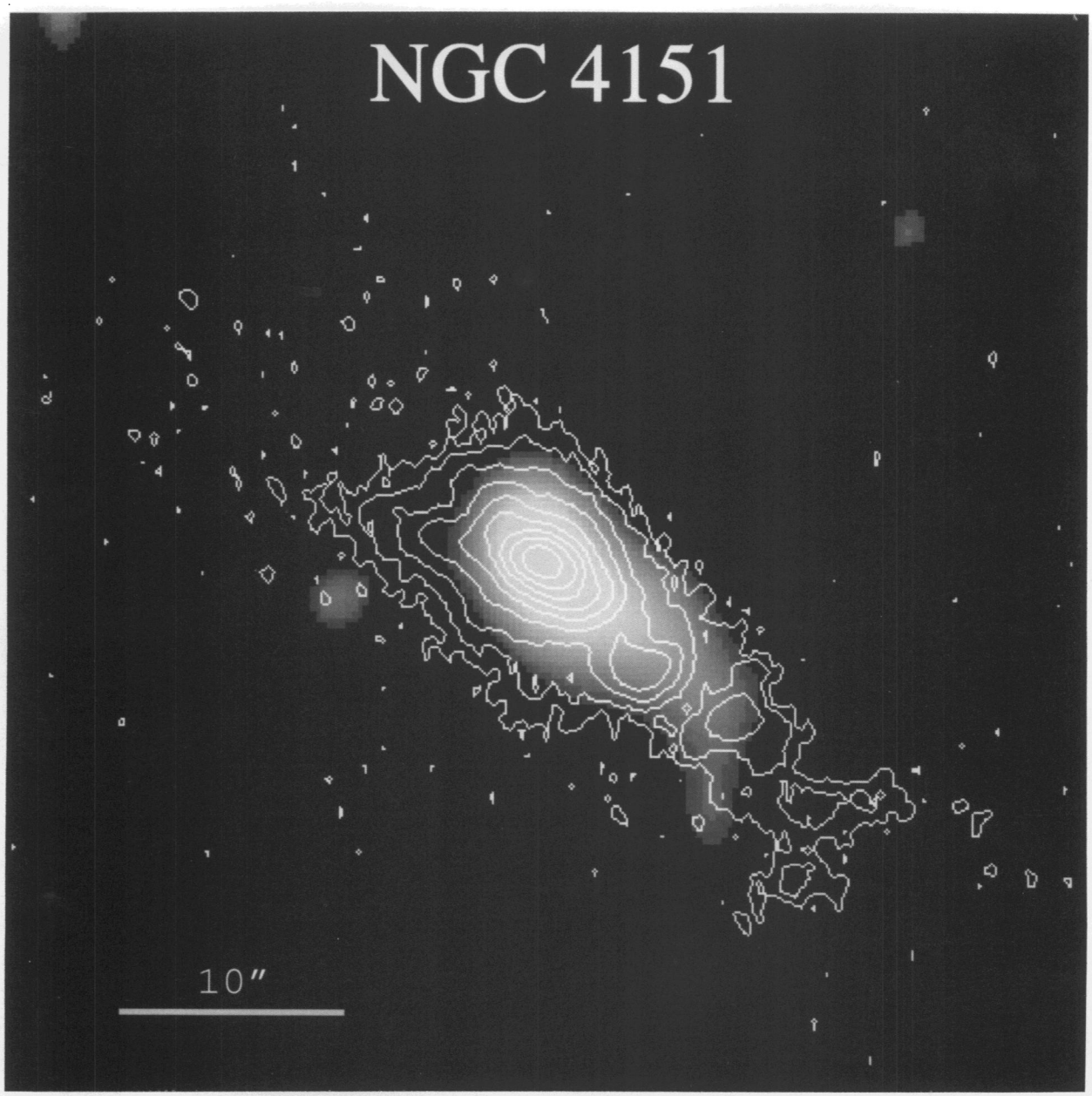

FIG. 9.—The gray scale is the deconvolved HRI image of NGC 4151. Contours of the optical [O III] emission from the image of Pérez-Fournon & Wilson (1990) are overlayed. The peak intensities of the two images were assumed to align. North is to the top and east is to the left.

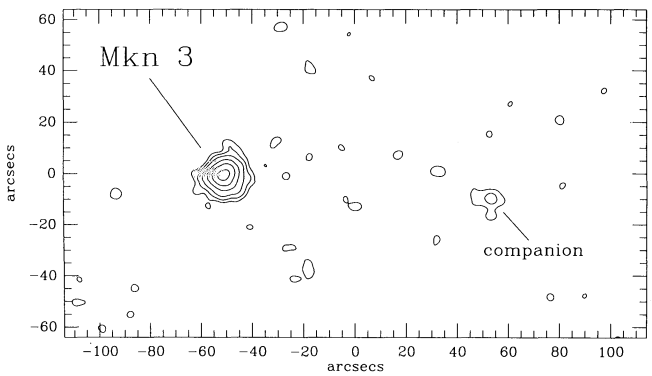

FIG. 10.—Contour diagram of the HRI image of Mrk 3 and its faint X-ray companion. The X-ray contours are set to 2.5%, 5%, 10%, 25%, 50%, and 85% of the maximum intensity in Mrk 3. The companion lies along PA ~ 265°, closely aligned with the axis of the 2″ bipolar nuclear radio jet (PA ≈ 84°/264°), though its physical association with Mrk 3 is uncertain.

Mrk 3 is very faint in our *ROSAT* HRI image. Nevertheless, we did attempt to correct for possible systematic offsets between the individual OBIs due to aspect errors. Separate subimages were created from eight OBIs, ranging in duration from ~2100 s to ~2700 s. While there were no obvious large OBI-to-OBI spatial offsets between the separate subimages, several of the subimages were multipeaked, presumably because of poor photon statistics and/or aspect errors during the satellite wobble. Each subimage was smoothed by a Gaussian with FWHM of 4″ and the location of each centroid was measured. Positions measured in multipeaked subimages were not necessarily centered on the brightest pixel but represented a local "average" centroid. We then aligned the subimages and co-added them into a single image, the result appearing in Figure 10.

The azimuthally averaged radial brightness profile of the corrected image of Mrk 3 is shown in Figure 11. The Mrk 3 profile is somewhat broadened compared to the original HZ 43 observation, but the profile is still typical of an unresolved point source blurred by aspect errors (David et al. 1993). In addition, there are no obvious elongations in the image (Fig. 10). We conclude that Mrk 3 is probably unresolved.

Turner, Urry, & Mushotzky (1993) noticed an excess of serendipitous X-ray sources near several Seyfert 2 galaxy nuclei, including Mrk 3. We also detect the faint X-ray companion to Mrk 3 (Fig. 10) discovered by Turner et al. (1993). Assuming that the X-rays we observe from Mrk 3 are centered on the unresolved nucleus, the X-ray companion is offset 104″ west and 9″ south from the nucleus, which is within a couple of arcseconds of the relative position given by Turner et al. (1993). This places the companion at $\alpha = 06^h15^m15^s.1$, $\delta = +71°02'04''$ (J2000), adopting the coordinates of the nucleus given by Kukula et al. (1993). The companion lies along PA 265° ± 2° with respect to the nucleus and is closely aligned with the axis of the 2″ radio jet (PA ≈ 84°/264°; Kukula et al 1993). Turner et al. (1993) report a luminosity for the companion of $\sim 2 \times 10^{40}$ ergs s^{-1} if it is at the distance of Mrk 3, too low for an AGN or BL Lac object. These authors identify a candidate optical counterpart at the detection limit of the POSS E plate at $\alpha = 06^h15^m11^s.2$, $\delta = +71°01'58''.2$ (J2000), some 20″ from the X-ray companion. Because our two relative positions for the X-ray companion agree to within a couple of arcseconds and our absolute position should be accurate to a few arcseconds, we conclude that the putative optical counterpart is not related to the X-ray companion. The X-ray companion may be a foreground or background source, but Turner et al. estimate that, given the absence of an optical counterpart on the POSS E plate, the X-ray-to-optical flux ratio is too high for the companion to be a star. The close alignment with the radio jet axis may suggest the companion X-ray source has been ejected from the nucleus of Mrk 3. If so, the companion is at a projected distance of ~40 kpc from the nucleus.

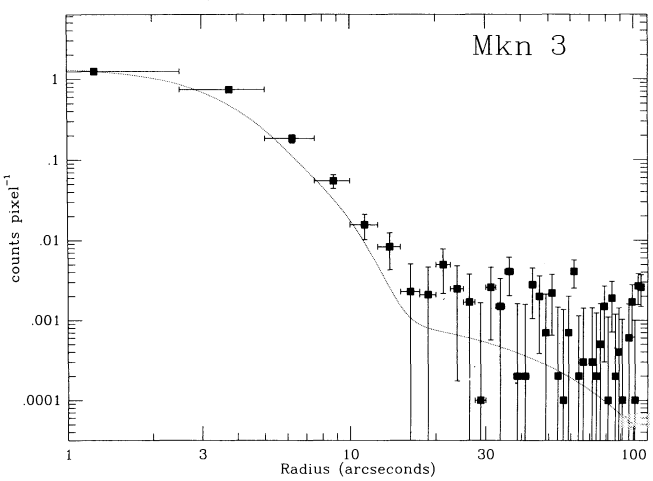

FIG. 11.—The azimuthally averaged radial brightness profile of Mrk 3. The dotted line is the scaled fit to the original HZ 43 image from Fig. 1.

2.3. *HRI Pulse Height Spectra*

The HRI has a limited spectral capability, but at present the energy response of the HRI is not calibrated well enough to permit modeling of spectra. We can, however, distinguish the relative hardness of spectra by calculating a "hardness ratio," formed by dividing the number of counts in PHA channels 5–10 by the number of counts in channels 1–4 (see David et al. 1993). Harder spectra have higher hardness ratios. Figure 12 compares the background-subtracted pulse height spectra over the 15 HRI energy channels for the three Seyfert galaxies plus BL 1207+39. All of the pulse height distributions are inconsistent with a signal deriving completely from UV leakage in the HRI, for which the counts would appear primarily in the first two channels.

Table 1 lists the hardness ratios for the sources we observed. The hardest source in this sample is Mrk 3, while the softest is NGC 4151. We also calculated hardness ratios in the southwest quadrant of NGC 4151 for the image core and extended emission separately. The hardness ratio inside a radius of 5″ equals 0.23 ± 0.04, while between radii of 5″ and 15″ the ratio is 0.27 ± 0.04. The present observation is consistent with no change in the hardness ratio as a function of radius along the southwest extension. A much deeper image is necessary to improve the photon statistics beyond 5″ from the source center.

2.4. *HRI Fluxes*

Soft X-ray fluxes can be estimated from HRI images if the spectrum is completely specified, save for the normalization. For simplicity, we measured 0.1–2 keV fluxes from our HRI images using power law plus absorption and thermal bremsstrahlung plus absorption spectra as input models. The soft X-ray spectra in these sources generally require more detailed

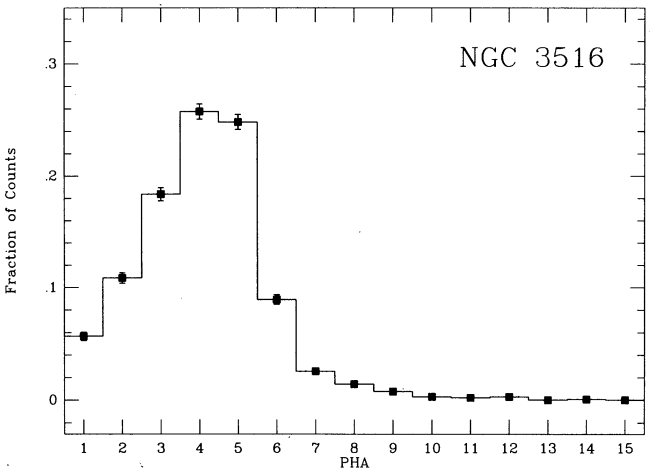

FIG. 12*a*

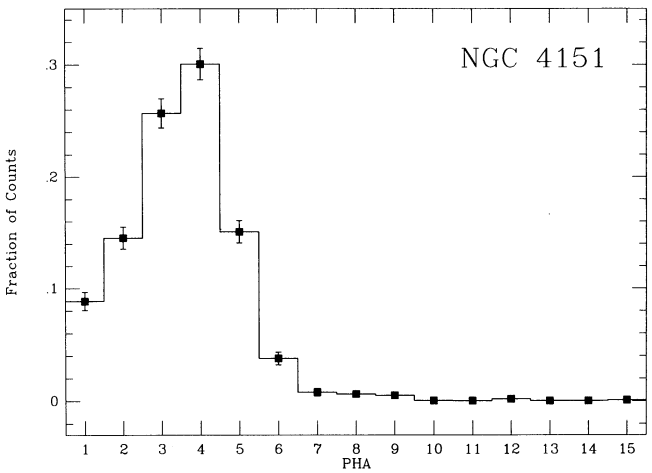

FIG. 12*b*

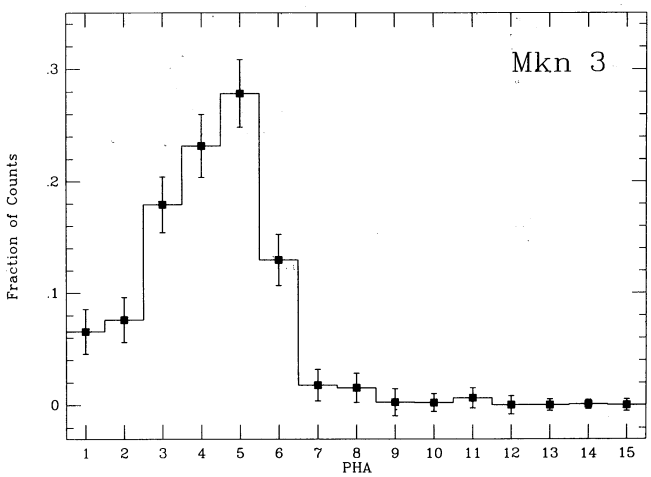

FIG. 12*c*

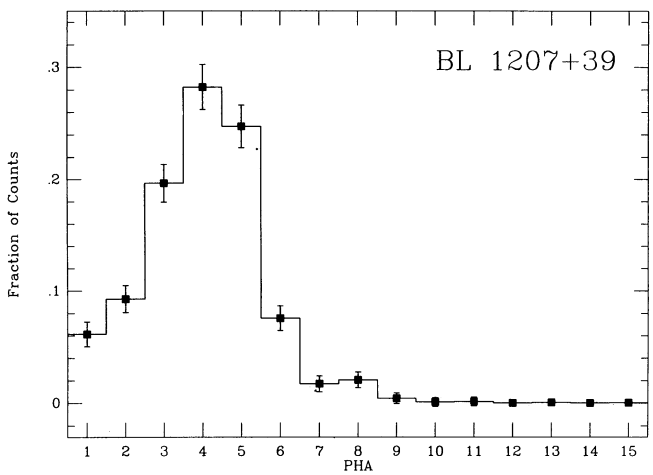

FIG. 12*d*

FIG. 12.—Observed pulse height distributions

models (e.g., see Weaver et al. 1994a), but the limited spectral resolution of the HRI renders such complex models unnecessary. We preferentially employed spectral fits determined from *ROSAT* PSPC observations of each source, if such measurements were available, because of the similar energy responses of the two instruments. All of the Seyfert galaxies have heavily absorbed, hard nuclear spectra above 2 keV (e.g., Ghosh & Soundararajaperumal 1991; Perola et al. 1986; Yaqoob & Warwick 1991; Yaqoob et al. 1993; Weaver et al. 1994*a*; Awaki et al. 1990; Marshall et al. 1991).

No *ROSAT* PSPC spectrum of NGC 3516 is available, so we used the power-law fit determined by Kruper, Urry, & Canizares from *Einstein* IPC observations. For NGC 4151 and BL 1207+39, we fitted a 38 ks PSPC observation available in the *ROSAT* archive. Both sources in this observation are noticeably elongated, presumably because of aspect errors, and our PSPC fluxes may be somewhat underestimated. The power-law fits to each source spectrum have moderately steep spectral indices and reasonable intrinsic absorption. In contrast, for Mrk 3 we used the mean power-law fit to two PSPC observations obtained by Turner et al. (1993), who measured a very steep spectrum with considerable intrinsic absorption.

Table 2 lists the measured HRI fluxes and those from the PSPC where available. The soft X-ray fluxes we measure from the HRI images tend to be higher than those measured from the PSPC. Reasons for the discrepancy may include intrinsic variability in the soft X-ray fluxes (e.g., see Ghosh & Soundararajaperumal 1991), a systematic offset in the flux calibration of the HRI, or possibly some UV leakage in the first two PHA channels (see David et al. 1993).

3. THE EXTENDED X-RAY EMISSION IN NGC 4151

The detection of extended X-rays in NGC 4151 seems secure, in agreement with the results of Elvis et al. (1983). In our deconvolved images of NGC 4151 (with and without a central point source subtracted), we trace the extended X-rays along a position angle of $\sim 50°/230°$ as far as $\sim 15''$ southwest and $\sim 5''$ northeast of the nucleus. At least 31% of the HRI flux from NGC 4151 is spatially extended and is cospatial with the optical ENLR. For either a power-law or thermal bremsstrahlung description of the emission, the flux of the spatially extended emission is $F(0.1\text{–}2\ \text{keV}) \approx 2.5 \times 10^{-12}$ ergs s^{-1} cm^{-2}, which corresponds to an unabsorbed luminosity of $L(0.1\text{–}2\ \text{keV}) \sim 3 \times 10^{41}$ ergs s^{-1}. It is also possible that much of the emission that is *unresolved* at the $\sim 5''$ FWHM resolution of the HRI is extended on scales of the NLR (10–100

TABLE 2

ROSAT SOFT X-RAY FLUX MEASUREMENTS

	Power Law				Bremsstrahlung					
Object	α[a]	N_H[b]	F_{PSPC}[c]	F_{HRI}[c]	kT[d]	N_H[b]	F_{PSPC}[c]	F_{HRI}[c]	D[e]	L[f]
NGC 3516[g]	0.60	1.6	...	13.9	0.5	3.0	...	13.8	55	6.7
NGC 4151	1.55	3.1	5.1	8.1	0.8	1.7	4.8	7.7	20	0.9
Mrk 3[h]	3.58	39.7	0.6	0.9	0.5	8.7	...	1.0	80	1.1
BL 1207+39.....	1.10	3.3	2.1	4.4	...	...	...	...	4160	1.8

[a] Energy index, $F_E \propto E^{-\alpha}$.

[b] Neutral hydrogen column densities are given in units of 10^{20} cm^{-2}. Only Galactic absorption was assumed for bremsstrahlung fits.

[c] Observed 0.1–2 keV fluxes in units of 10^{-12} ergs cm^{-2} s^{-1}.

[d] In keV.

[e] Distance to object in Mpc, assuming $H_0 = 50$ km s^{-1} Mpc^{-1} and $q_0 = 0.5$.

[f] Total unabsorbed 0.1–2 keV HRI luminosity from power-law fits in units of 10^{42} ergs s^{-1}. For BL 1207+39, L is in units of 10^{46} ergs s^{-1}.

[g] *ROSAT* PSPC spectrum not available. The power-law model was derived by Kruper et al. 1990 from *Einstein* IPC observations. The bremsstrahlung fit to the HRI data assumes a temperature of $kT = 0.5$ keV and a Galactic column density of 3.0×10^{20} cm^{-2}.

[h] PSPC power law fit from Turner et al. 1993. The bremsstrahlung fit to the HRI data assumes a temperature of $kT = 0.5$ keV and a Galactic column density of 8.7×10^{20} cm^{-2} as used by Turner et al. 1993.

pc). The flux from the extended, resolved regions that we observe with the HRI [F(0.2–1 keV) $\sim 1.6 \times 10^{-12}$ ergs s^{-1} cm^{-2}] accounts for roughly half of the soft excess observed with other X-ray detectors [e.g., F(0.2–1 keV) $\approx 2.8 \times 10^{-12}$ ergs s^{-1} cm^{-2}, Weaver et al. 1994*a*; F(0.2–1 keV) $\approx 4.0 \times 10^{-12}$ ergs s^{-1} cm^{-2}, Pounds et al. 1986]. X-ray spectral monitoring of NGC 4151 (e.g., Perola et al. 1986), including several *ASCA* observations (Weaver et al. 1994c), suggests that the soft X-ray excess contains distinct flux components, one that varies with time and one that stays constant, each component contributing about 50% of the flux below ~ 1 keV. The *ROSAT* HRI is most sensitive to the energies where the soft X-ray excess is seen, and the HRI flux we observe in the extended regions is consistent with that observed for the constant spectral component. We thus suggest that the constant flux component originates from the circumnuclear environment that projects as far as ~ 0.5 kpc northeast and ~ 1.5 kpc southwest of the nucleus. Similarly, Weaver et al. (1994b) propose that the soft excess seen in the Seyfert 2 galaxy NGC 2110 is the same component as the spatially extended emission resolved in their HRI image.

There are several mechanisms that could, in principle, produce the observed soft X-ray emission distribution in NGC 4151. The close spatial correspondence between the extended optical emission-line and soft X-ray structures suggests a common or related origin. Determining whether the soft X-ray spectrum hardens or softens as a function of radius along the extent could help to discriminate between various models (e.g., as in NGC 1068; Wilson et al. 1992). Unfortunately, the signal-to-noise ratios in the present HRI observation are not adequate in the extended regions to measure reliably the spatial dependence of the hardness ratio.

The extended X-rays may be electron-scattered nuclear photons. Weaver et al. (1994a) found that a fraction $f_{scatt} \simeq 0.03$–0.06 of the unabsorbed hard nuclear spectrum needs to be scattered to account for the flux in the soft excess, depending on whether the hard spectrum is in a high state or low state. Here we adopt an average scattered fraction of $f_{scatt} = 0.045$, of which $\sim 61\%$ (or 0.027) comes from the southwest extension. We can then calculate the optical depth to Thomson scattering in the southwest region using $\tau_{es} = f_{scatt}(\Omega/4\pi)^{-1}$, where Ω is the solid angle subtended by the scattering medium at the nuclear source, assuming the central source radiates isotropically. The full opening angle of the ionization bicone is $\sim 75°$ (Evans et al. 1993) corresponding to a solid angle $\Omega/4\pi = 0.10$ sr (for one side of the bicone). The optical depth $\tau_{es} = 0.28$ and the radial column density of material in the scattering zone $N_{es} = \tau_{es}/\sigma_T = 4.1 \times 10^{23}$ cm^{-2}. The radial extent along the southwest quadrant is ~ 1.5 kpc, yielding a volume density of $n_{SW} = 88$ cm^{-3}. A similar calculation for the northeast quadrant gives $f_{scatt} \sim 0.017$, $\tau_{es} = 0.17$, $N_{es} = 2.4 \times 10^{23}$ cm^{-2}, and a volume density over the ~ 0.5 kpc extension of $n_{NE} = 155$ cm^{-3}. For uniformly filled cones, the combind mass of gas is an implausible $5 \times 10^9 M_\odot$.

The gas in the scattering medium must be highly stripped in order for the soft X-rays to escape (Krolik & Kallman 1984). Elvis et al. (1990) show that is is difficult to achieve this through collisions without thermal bremsstrahlung emission dominating the scattered radiation. Assuming then that the medium is photoionized by the nuclear continuum (e.g., Pérez-Fournon & Wilson 1990; Robinson et al. 1994), we can derive the central source luminosity needed to render the scattering zone transparent to ~ 1 keV X-rays. The ionization structure of an optically thin gas is determined by the ionization parameter $\xi = L/nR^2$, where L is the luminosity of ionizing radiation from the central source, and n is the gas density at a distance R from the central source. For gas in photoionization equilibrium to be transparent to 1 keV X-rays, the ionization parameter ξ needs to be greater than 73 ($\Xi > 14$; Krolik & Kallman 1984), assuming a power-law ionizing continuum with an index of -1. To reach this level of ionization along the southwest extension requires a central source luminosity of $L \approx 3 \times 10^{46}$ ergs s^{-1} in the 0.1–2 keV bandpass. This is over four orders of magnitude greater than the total unabsorbed 0.1–2 keV luminosity we observe (Table 2). We conclude that if the extended soft X-rays represent scattered nuclear X-rays, the source photons must be radiated preferentially toward the scattering zone. Incorporating such anisotropy into the scattering model, f_{scatt}(anisotropic) $= (L_E/L_S) f_{scatt}$(isotropic), where L_E and L_S are the luminosities emitted toward Earth and the scattering zone, respectively. This relation reduces the necessary scattering column significantly from the isotropic case and

yields a more plausible value of L_S. The anisotropy needed in the scattering model may be related to that inferred from the optical observations (Pérez-Fournon & Wilson 1990; Evans et al. 1993).

The close association of the extended soft X-rays with the extended forbidden-line gas in NGC 4151 suggests that the X-rays may arise from hot gas in pressure equilibrium with the ENLR (Heckman & Balick 1983). Krolik & Vrtilek (1984) present a picture in which the cool optical emission-line clouds are entrained by a hot nuclear wind. These clouds are expected to be in rough pressure equilibrium with the surrounding hot intercloud medium (ICM), such that $n_{\rm cl} T_{\rm cl} \approx n_{\rm ICM} T_{\rm ICM}$. Penston et al. (1990) derived emissivity-weighted estimates for the electron density and electron temperature in the southwest optical ENLR of $n_e \approx 220$ cm^{-3} and $T_e \approx 14130$ K, corresponding to a pressure of $n_e T_e = 3.1 \times 10^6$ cm^{-3} K. For a temperature in the hot gas of $T_{\rm ICM} \sim 10^7$ K (Table 2; Weaver et al. 1994a), the inferred density in the ICM is $n_{\rm ICM} = 0.3$ cm^{-3}. The total X-ray luminosity from thermal emission in the 0.1–2 keV energy range for a hot plasma occupying the volume subtended by the southwest extended X-rays with $T = 10^7$ K, $n = 0.3$ cm^{-3} and cosmic abundances, as calculated using the thermal X-ray emission code XSPCT developed by J. Raymond (CfA), is $L_{\rm th} = 1.9 \times 10^{41}$ ergs s^{-1}, which agrees with the unabsorbed luminosity of $\sim 1.7 \times 10^{41}$ ergs s^{-1} that we observe. The NLR clouds have a characteristic size of $\sim 0''.2$ ($= 20$ pc), and their kinematics indicate they are flowing out from the nuclear vicinity (Evans et al. 1993; Boksenberg et al. 1994). In addition, Schultz (1988) detected two velocity components in the ENLR, suggesting that at least some of the line-emitting material in the ENLR is moving anomalously with respect to the galactic rotation. Moving at ~ 200 km s^{-1} with respect to the ambient medium, the clouds can traverse the southwest extended region in a time $t_{\rm cross} \approx 8 \times 10^6$ yr (correcting for an inclination to the line of sight of $\phi \sim 65°$ for the cone axis; Evans et al. 1993). By comparison, the evaporation timescale for such a cloud is $t_{\rm evap} \simeq 2.5 \times 10^7$ yr, using equation (22) of Cowie & McKee (1977) which applies to the classical case. If there is a large relative velocity between the clouds and the hot gas—for instance, if the clouds are entrained near the nucleus and are then accelerated by the ram pressure of the fast, hot wind—the clouds can be destroyed by dynamical instabilities. The cloud disruption timescale due to the Rayleigh-Taylor instability is estimated as (e.g., Allen 1984)

$$t_{\rm RT} \sim \left(\frac{R_{\rm cl}}{V_{\rm rel}}\right) \eta^{1/2} ,$$

where $R_{\rm cl}$ is the cloud radius, $V_{\rm rel}$ is the relative velocity between the cloud and the hot gas, and η is the cloud-to-intercloud gas density ratio. Using a cloud radius of 10 pc, a relative velocity of 200 km s^{-1}, and a density ratio of $\eta \approx 733$, the disruption timescale is $t_{\rm RT} \sim 1.3 \times 10^6$ yr, somewhat shorter than $t_{\rm cross}$. However, this estimate is based on a linear perturbation analysis and has been shown to be too low in certain instances. For example, Knerr (1993) showed in numerical simulations that wind-accelerated clouds maintain their cohesion much longer than the disruption timescale $t_{\rm RT}$ because cloud ablation by the hot wind gas limits the growth of surface instabilities along the cloud boundary. The values for $t_{\rm RT}$ and $t_{\rm evap}$ are comparable to $t_{\rm cross}$, and given these order-of-magnitude calculations, this suggests that cool forbidden-line clouds could survive for a crossing time in rough pressure equilibrium with the hot intercloud medium.

4. SUMMARY

Extended soft X-rays have been detected in a *ROSAT* HRI image of NGC 4151, confirming the results of Elvis et al. (1983). We have deconvolved our images of NGC 4151 (both with and without a central point source subtracted), and can trace the extended X-rays along a position angle of $\sim 50°/230°$ as far as $\sim 15''$ (1.5 kpc) southwest and $\sim 5''$ (0.5 kpc) northeast of the nucleus. The extended emission accounts for at least 31% of the total 0.1–2 keV flux observed and constitutes roughly half of the total soft X-ray excess emission seen with other X-ray detectors. We have considered both electron-scattering and thermal emission as origins for the extended X-rays. If the extended X-rays represent electron-scattered nuclear X-rays, the central source must emit preferentially toward the scattering region. Alternatively, the extended X-rays may result from thermal emission by a hot ($T \sim 10^7$ K), low-density ($n_e \lesssim 1$ cm^{-3}), outflowing wind which is in rough pressure equilibrium with the optical narrow line-emitting clouds on the same spatial scale. Without spatially resolved X-ray spectra and information on the temporal variability of the extended flux, it is difficult to assess which model for the extended X-rays is more plausible. However, associating the extended X-rays we resolve with the constant flux component of the soft X-ray excess (Perola et al. 1986) and combining this with the presence of outflowing emission-line clouds in the same region (Schultz 1988), leads us to favor the thermal emission model for the extended X-ray emission over the scattering picture.

Our HRI image of NGC 3516 shows an elongation along a position angle of $\sim 40°/220°$ that aligns with the Z-shaped NLR, although residual aspect errors render the reality of this extension questionable. Mrk 3 is very faint in our HRI image and is probably unresolved. We do detect the faint X-ray source $\sim 2'$ west of the Mrk 3 nucleus previously found by Turner et al. (1993). It is not known whether this companion is physically associated with Mrk 3, although it does lie along a direction that is within $\sim 1°$ of the axis of the $2''$ nuclear radio jet. We also detected the BL Lac object BL 1207+39 $\sim 5'$ north-northwest of NGC 4151. There is some suggestion of excess X-ray emission in the azimuthally averaged radial brightness profile of BL 1207+39 between radii of $10''$ and $30''$ when compared to a calibration source, though a much deeper image is necessary to confirm this result.

We are indebted to the *ROSAT* support staffs at SAO, MPE, and GSFC for their help with the data reduction and analysis. We appreciate the valuable discussions with G. Cecil, L. David, D. Harris, G. Hasinger, J. Knerr, J. Krolik, F. D. Machetto, A. Schiano, Q. Wang, and M. Zombeck. We also thank Skip Westphal, John Bedke, and the rest of the STScI Photolab crew for their expert assistance in producing Figures 8 and 9. This work has been supported at STScI by NASA grants NAGW-2689 and NAGW-3268, and at the CfA by NASA grant NAGW-2201 (LTSA).

REFERENCES

Allen, A. J. 1984, MNRAS, 210, 147
Awaki, H., Koyama, K., Kunieda, A., & Tawara, Y. 1990, Nature, 346, 544
Boksenberg, A., et al. 1994, A&A, submitted
Cecil, G., Wilson, A. S., & DePree, C. 1994, ApJ, submitted
Cowie, L. L., & McKee, C. F. 1977, ApJ, 211, 135
David, L. P., Harnden, F. R., Jr., Kearns, K. E., & Zombeck, M. V. 1993, The *ROSAT* High Resolution Imager (HRI) (Technical Rep., US *ROSAT* Science Data Center/SAO)
Elvis, M., Briel, U. G., & Henry, J. P. 1983, ApJ, 268, 105
Elvis, M., Fassnacht, C., Wilson, A. S., & Briel, U. 1990, ApJ, 361, 459
Evans, I. N., Tsvetanov, Z., Kriss, G. A., Ford, H. C., Caganoff, S., & Koratkar, A. P. 1993, ApJ, 417, 82
Ghosh, K. K., & Soundararajaperumal, S. 1991, ApJ, 383, 574
Goad, J. W., & Gallagher, J. S., III 1987, AJ, 94, 640
Haniff, C. A., Wilson, A. S., & Ward, M. J. 1988, ApJ, 334, 104
Heckman, T. M., & Balick, B. 1983, ApJ, 268, 102
Knerr, J. M. 1993, Ph.D. thesis, Univ. North Carolina
Krolik, J. H., & Kallman, T. R. 1984, ApJ, 286, 366
Krolik, J. H., & Vrtilek, J. M. 1984, ApJ, 279, 521
Kruper, J. S., Urry, C. M., & Canizares, C. R. 1990, ApJS, 74, 347
Kukula, M. J., Ghosh, T., Pedlar, A., Schilizzi, R. T., Miley, G. K., de Bruyn, A. G., & Saikia, D. J. 1993, MNRAS, 264, 893
Marshall, F. E., et al. 1991, in Frontiers of X-ray Astronomy, Proc. 28th Yamada Meeting, Nagoya, Japan, ed. Y. Tanaka & K. Koyama (Tokyo: Universal Academy Press), 233
Miller, J. S., & Goodrich, R. W. 1990, ApJ, 355, 456
Miyaji, T., Wilson, A. S., & Pérez-Fournon, I. 1992, ApJ, 385, 137
Morse, J. A. 1994a, PASP, 106, 675
———. 1994b, in The Soft X-ray Cosmos: Proc. *ROSAT* Science Symposium, ed. R. Petre & E. M. Sclegel (AIP: New York), 252
Mulchaey, J. S., Tsvetanov, Z., Wilson, A. S., & Pérez-Fournon, I. 1992, ApJ, 394, 91
Penston, M. V., et al. 1990, A&A, 236, 53
Pérez-Fournon, I., & Wilson, A. S. 1990, ApJ, 356, 456
Perola, G. C., et al. 1986, ApJ, 306, 508
Pogge, R. W. 1989, AJ, 98, 124
Pounds, K. A., Warwick, R. S., Culhane, J. L., & de Korte, P. A. J. 1986, MNRAS, 218, 685
Robinson, A., et al. 1994, A&A, in press
Schmitt, J. H. M. M., Güdel, M., & Predehl, P. 1994, A&A, in press
Schultz, H. 1988, A&A, 203, 233
Turner, T. J., Urry, C. M., & Mushotzky, R. F. 1993, ApJ, 418, 653
Veilleux, S., Tully, R. B., & Bland-Hawthorn, J. 1993, AJ, 105, 1318
Weaver, K. A., Mushotzky, R. F., Arnaud, K. A., Serlemitsos, P. J., Marshall, F. E., Petre, R., Jahoda, K. M., Smale, A. P., & Netzer, H. 1994a, ApJ, in press
Weaver, K. A., Mushotzky, R. F., Serlemitsos, P. J., Wilson, A. S., Elvis, M., & Briel, U. G. 1994b, in preparation
Weaver, K. A., et al. 1994, in preparation
Wilson, A. S. 1994, in The Soft X-ray Cosmos: Proc. *ROSAT* Science Symposium, ed. R. Petre & E. M. Sclegel (AIP: New York), in press
Wilson, A. S., Elvis, M., Lawrence, A., & Bland-Hawthorn, J. 1992, ApJ, 391, L75
Wrobel, J., & Heeschen, D. S. 1988, ApJ, 335, 677
Yaqoob, T., & Warwick, R. S. 1991, MNRAS, 248, 773
Yaqoob, T., Warwick, R. S., Makino, F., Otani, C., Sokoloski, J. L., Bond, I. A., & Yamauchi, M. 1993, MNRAS, 262, 435
Zombeck, M. V., Conroy, M., Harnden, F. R., Roy, A., Braeuninger, H., Burkert, W., Hasinger, G., & Predehl, P. 1990, in Proc. SPIE Conference on EUV, X-Ray and Gamma-Ray Instrumentation for Astronomy, ed. O. H. W. Siegmund & H. S. Hudson (SPIE Proc., 1344), 267